Quantum-Enhanced Stimulated Brillouin Scattering Spectroscopy and Imaging Supplementary Material

Tian Li,[1,2,*] Fu Li,[1,3] Xinghua Liu,[1,3] Vladislav V. Yakovlev,[3,4,5] and Girish S. Agarwal[1,2,3]

[1] *Institute for Quantum Science and Engineering, Texas A&M University, College Station, TX 77843, USA*
[2] *Department of Biological and Agricultural Engineering, Texas A&M University, College Station, TX 77843, USA*
[3] *Department of Physics and Astronomy, Texas A&M University, College Station, TX 77843, USA*
[4] *Department of Biomedical Engineering, Texas A&M University, College Station, TX 77843, USA*
[5] *Department of Electrical and Computer Engineering, Texas A&M University, College Station, TX 77843, USA*

I. EXPERIMENTAL DETAILS

A. Experimental Setup Description

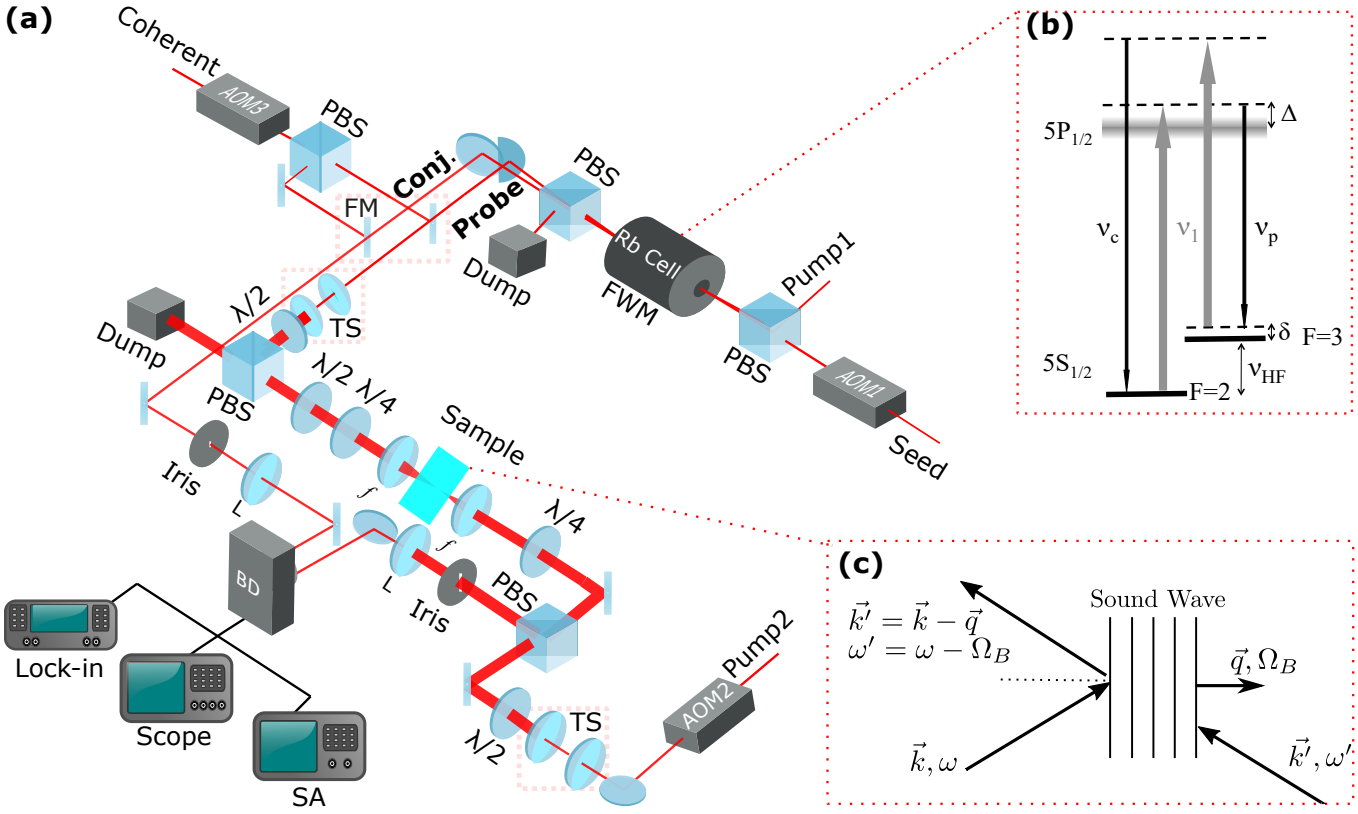

FIG. 1. (a) Experimental setup. See text for a detailed description. L: lens, FM: flip mirror, TS: telescope, PBS: polarizing beam splitter, BD: balanced detector, SA: RF spectrum analyser. (b) Level structure of the D1 transition of ^{85}Rb atom. The optical transitions are arranged in a double - Λ configuration, where ν_p, ν_c and ν_1 stand for probe, conjugate and pump frequencies, respectively, fulfilling $\nu_p + \nu_c = 2\nu_1$ and $\nu_c - \nu_p = 2\nu_{HF}$. The width of the excited state in the level diagram represents the Doppler broadened line. Δ is the one-photon detuning. $\nu_{\rm HF}$ is the hyperfine splitting in the electronic ground state of ^{85}Rb. (c) Phase-matching diagram for the SBS process [1]. The wave-vectors and frequencies for the pump, probe and sound wave are denoted by $(\vec{k}, \omega)$, $(\vec{k'}, \omega')$ and $(\vec{q}, \Omega_B)$ respectively.

* tian.li@tamu.edu

The atomic medium is pumped by a strong ($\sim$ 500 mW) narrow-band continuous-wave (CW) laser (shown in Fig. 1(a) as "Pump 1") at frequency ν_1 (λ = 795 nm) with a typical linewidth $\Delta\nu_1 < 1$ MHz. Applying an additional weak (in the range of a few hundreds μW) coherent beam (shown in Fig. 1(a) as "Seed") at frequency $\nu_p = \nu_1 - (\nu_{HF} + \delta)$, where ν_{HF} and δ are the hyperfine splitting in the electronic ground state of ^{85}Rb and the two-photon detuning ($\delta = 5$ MHz in this work) respectively in Fig. 1(b) (further experimental details can be found in Ref. [2]), two pump photons are converted into a pair of twin photons, namely 'probe ν_p' and 'conjugate ν_c' photons, adhering to the energy conservation $2\nu_1 = \nu_p + \nu_c$ (see the level structure in Fig. 1(b)). The resulting twin beams are strongly quantum-correlated and are also referred to as bright two-mode squeezed light [3]. The twin beams exhibit a intensity-difference squeezing of 6.5 dB measured by a balanced detector (with customized photodiodes having 94 % quantum efficiency at 795 nm, further squeezing measurement details can be found in Ref. [2]), which is indicative of strong quantum correlations [3].

After the ^{85}Rb vapor cell, the pump and the twin beams (shown in Fig. 1(a) as "Probe" and "Conj.") are separated by a Glan-Laser polarizer, with $\sim 2 \times 10^5 : 1$ extinction ratio for the pump. The probe beam then passes through a telescope (TS) with an enlarged beam waist ($\sim$ 3 mm) before focused (down to a $1/e^2$ beam waist of $\sim$ 5 μm by a plano-convex lens with focal length f = 16 mm) and overlapped with a counter propagating laser beam (shown in Fig. 1(a) as "Pump 2", a same type of CW laser as "Pump 1", and having a $1/e^2$ beam waist of $\sim$ 6 μm) at a homemade sample holder filled with distilled water, to form a phase-matching geometry for the SBS process in water depicted in Fig. 1(c). The sample holder consists of two glass microscope slides separated by 1 mm with water filled between them. Both $\lambda/2$ and $\lambda/4$ waveplates are added in the probe beam path in order for the probe beam to be reflected as much as possible by the polarizing beam splitter (PBS) into one port of the balanced detector (BD). Therefore in this configuration, the probe beam is linearly polarized while the pump beam for the SBS process ("Pump 2" in Fig. 1(a)) is circularly polarized. The conjugate beam serves as a reference, and two flip mirrors (FM) are used for the introduction of two coherent beams so that the whole setup can be converted into a classical version. The pumps and probe beams are amplitude-modulated by three AOMs at 300 KHz (AOM1) and 400 KHz (AOM2&3) respectively. The water SBS signal therefore is expected to appear at 700 KHz where the two-mode squeezing is expected to be the best [2, 4]. The balanced detection uses two coherent beams and a balanced detector, which subtracts away common-mode noise to better than 25 dB, therefore contributions from low-frequency technical noise can be eliminated, so that the noise level at the modulation frequency (where the signal occurs) would be (or close to) shot-noise limited. There is no contribution from the stray pump light to the detection noise as there is a decent angle separation ($\sim$ 0.3°) between the twin beams and the pump beam, and there are multiple irises in the paths of the twin beams to filter out the stray pump light.

In addition to the components shown in Fig. 1(a), there are also frequency-locking optics and electronics for the probe and pump beams of the SBS process so that they can be locked and separated by the phonon frequency $\Omega_B/2\pi$ (or so-called "Brillouin frequency shift") of water, which is in the range of $\sim$ 5 GHz [5]. In this work, we use fringes from a room temperature Fabry-Perot cavity as the locking error signal and absorption lines from a room temperature natural abundant Rb cell as the locking reference for each laser beam. We change the frequency difference between the two beams by fixing the probe frequency (at one photon detuning $\Delta \sim 1$ GHz shown in Fig. 1(b)) so that the FWM process can yield the best two-mode squeezing, while scanning the locking frequency of the pump with a minimal step of 40 MHz (determined by the resolution of the scanning voltage).

It is very important to point out that in our scheme, we used a "two-mode" squeezed state, where squeezing resides in the "intensity-difference" between the two involving modes. As opposed to the experimental complexity of a single-mode squeezed scheme where a homodyne measurement is needed to characterize the squeezing, and a phase-locking mechanism is needed to track the squeezed quadrature, our scheme only requires a balance detector so that an intensity-difference measurement can be obtained. Therefore a "balanced coherent detection" where two coherent beams are used would be the appropriate classical counterpart to the quantum configuration in our scheme.

B. Microscopic Imaging Acquisition

The triangle-shaped glass used for imaging shown in the inset of Fig. 6(a) was made by cutting off a corner of a microscope slide whose thickness is 1 mm, and the lengths of the triangle's two sides are 7.5 mm and 6.5 mm respectively. Since our homemade sample holder consists of two glass microscope slides separated by 1 mm with water filled between them, the glass triangle therefore can be introduced into the sample holder so that there is no water content within the area of the triangle.

To acquire the images in Fig. 6 in the main text, we use two translational stages with differential micrometer screws to automatically move the sample holder's position with a spatial scan step size of 100 μm in both directions. The images are obtained by scanning each pixel under the experimental conditions shown in Fig. 3(b). Namely, the pump and probe powers are 7.5 mW and 750 μW respectively, and the two lasers are locked so that their frequency difference matches the 5 GHz Brillouin shift of water.

II. THEORETICAL FRAMEWORK

We use a single-mode quantum-mechanical model to simulate the experiment [6]. We denote the optical field operators for the probe and conjugate modes as $\hat{a}_{0,f}$ and $\hat{b}_{0,f}$ with subscripts 0 and f labeling the operators at the initial and final stages of transformation, respectively. The input-output relation for the FWM process, $\hat{a}_{\rm FWM} = (\cosh r)\hat{a} + (\sinh r)\hat{b}^\dagger$, where r is the squeezing operator, is well known. For the input-output relation for the SBS process, we can write it as $\hat{a}_{\rm SBS} = g\hat{a}_{\rm FWM} + \hat{F}$, where g is the SBS gain parameter, and $\hat{F}$ is the noise operator introduced by the SBS gain process. The field operator $\hat{a}_{\rm SBS}$ must satisfy the commutation relation $[\hat{a}_{\rm SBS}, \hat{a}^\dagger_{\rm SBS}] = 1$, from which the noise operator $\hat{F}$ can be derived as $\sqrt{g^2-1}\hat{\nu}^\dagger_{\rm B}$, where $\hat{\nu}_{\rm B}$ is a vacuum noise operator introduced by the SBS process. All optical and atomic absorption losses sustained by the twin beams are modeled by three beams splitters with transmission $\eta_{\rm p1}$, $\eta_{\rm p2}$ and $\eta_{\rm c}$ [7]. They represent the atomic and optical loss in the probe pathway between the FWM cell and the SBS sample holder ($\eta_{\rm p1}$), between the SBS sample holder and the balanced detector ($\eta_{\rm p2}$), and the optical loss in the conjugate pathway ($\eta_{\rm c}$), respectively. The experimentally measured values are $r = 1.39$ (which corresponds to our measured FWM gain of $\cosh^2 r = 4.5$), $\eta_{\rm p1} = 0.83$, $\eta_{\rm p2} = 0.75$ and $\eta_{\rm c} = 0.9$. Since we have kept all the noise operators, thus it is not the case of 'noiseless' amplification. Therefore this theoretical framework is not under the unitary condition. We treat all pump beams classically. The vectors $\hat{\vec{V}}_0$ and $\hat{\vec{V}}_f$ are the initial and final field operators defined by

$$\hat{\vec{V}}_0 = \begin{pmatrix} \hat{a}_0 \\ \hat{a}_0^\dagger \\ \hat{b}_0 \\ \hat{b}_0^\dagger \end{pmatrix} \quad \text{and} \quad \hat{\vec{V}}_f = \begin{pmatrix} \hat{a}_f \\ \hat{a}_f^\dagger \\ \hat{b}_f \\ \hat{b}_f^\dagger \end{pmatrix}. \tag{1}$$

The experiment can then be described by the transformation of field operators

$$\hat{\vec{V}}_f = \boldsymbol{T_2} \cdot \left(\boldsymbol{B} \cdot \left[\boldsymbol{T_1} \cdot (\boldsymbol{F} \cdot \hat{\vec{V}}_0) + \hat{\vec{L}}_1 \right] + \hat{\vec{L}}_B \right) + \hat{\vec{L}}_2, \tag{2}$$

where

$$\boldsymbol{F} = \begin{pmatrix} \cosh r & 0 & 0 & \sinh r \\ 0 & \cosh r & \sinh r & 0 \\ 0 & \sinh r & \cosh r & 0 \\ \sinh r & 0 & 0 & \cosh r \end{pmatrix}, \tag{3}$$

$$\boldsymbol{B} = \begin{pmatrix} g & 0 & 0 & 0 \\ 0 & g & 0 & 0 \\ 0 & 0 & 1 & 0 \\ 0 & 0 & 0 & 1 \end{pmatrix}, \tag{4}$$

and

$$\hat{\vec{L}}_B = \begin{pmatrix} \sqrt{g^2-1}\hat{\nu}^\dagger_{\rm B} \\ \sqrt{g^2-1}\hat{\nu}_{\rm B} \\ 0 \\ 0 \end{pmatrix}. \tag{5}$$

Matrix $\boldsymbol{F}$ describes the FWM process, while matrix $\boldsymbol{B}$ together with vector $\hat{\vec{L}}_B$ describe the SBS process. Matrices $\boldsymbol{T_1}$ and $\boldsymbol{T_2}$ describe the transmission of the beam splitters, and vectors $\hat{\vec{L}}_1$ and $\hat{\vec{L}}_2$ contain the field operators $\hat{\mu}_{\rm p1}$, $\hat{\mu}_{\rm p2}$ and $\hat{\mu}_{\rm c}$ for the vacuum noise coupled in by optical losses:

$$\boldsymbol{T_1} = \begin{pmatrix} \sqrt{\eta_{\mathrm{p1}}} & 0 & 0 & 0 \\ 0 & \sqrt{\eta_{\mathrm{p1}}} & 0 & 0 \\ 0 & 0 & 1 & 0 \\ 0 & 0 & 0 & 1 \end{pmatrix}, \tag{6}$$

$$\boldsymbol{T_2} = \begin{pmatrix} \sqrt{\eta_{\mathrm{p2}}} & 0 & 0 & 0 \\ 0 & \sqrt{\eta_{\mathrm{p2}}} & 0 & 0 \\ 0 & 0 & \sqrt{\eta_{\mathrm{c}}} & 0 \\ 0 & 0 & 0 & \sqrt{\eta_{\mathrm{c}}} \end{pmatrix}, \tag{7}$$

$$\hat{\vec{L_1}} = \begin{pmatrix} i\sqrt{1-\eta_{\mathrm{p1}}}\hat{\mu}_{\mathrm{p1}} \\ -i\sqrt{1-\eta_{\mathrm{p1}}}\hat{\mu}^{\dagger}_{\mathrm{p1}} \\ 0 \\ 0 \end{pmatrix}. \tag{8}$$

$$\hat{\vec{L_2}} = \begin{pmatrix} i\sqrt{1-\eta_{\mathrm{p2}}}\hat{\mu}_{\mathrm{p2}} \\ -i\sqrt{1-\eta_{\mathrm{p2}}}\hat{\mu}^{\dagger}_{\mathrm{p2}} \\ i\sqrt{1-\eta_{\mathrm{c}}}\hat{\mu}_{\mathrm{c}} \\ -i\sqrt{1-\eta_{\mathrm{c}}}\hat{\mu}^{\dagger}_{\mathrm{c}} \end{pmatrix}. \tag{9}$$

When a coherent state $|\beta\rangle$, $\beta = |\beta|e^{i\phi}$, where ϕ is the input phase, seeds mode a, and only vacuum fluctuations $|0\rangle$ seed mode b, then the input state can be written as $|\beta, 0, 0, 0, 0, 0\rangle$, where the last four zeros are inputs for the vacuum/noise operators $\hat{\nu}_{\mathrm{B}}$, $\hat{\mu}_{\mathrm{p1}}$, $\hat{\mu}_{\mathrm{p2}}$ and $\hat{\mu}_{\mathrm{c}}$ respectively. Although not trivial, it is fairly straightforward to calculate the number operators $\hat{n}_a = \hat{a}^{\dagger}_f\hat{a}_f$ and $\hat{n}_b = \hat{b}^{\dagger}_f\hat{b}_f$ for the probe and conjugate modes after detection, and the expectation values of quantities such as the noise suppression below the shot noise level, i.e. the quantum advantage:

$$\text{Quantum Advantage [dB]} = -10 \times \log_{10}\left[\frac{\Delta^2(\hat{n}_a - \hat{n}_b)}{\Delta^2\hat{n}_{\mathrm{SNL}}}\right], \tag{10}$$

where $\Delta^2\hat{n}_{\mathrm{SNL}}$ is the shot noise level, which is defined as the variance of the intensity difference of two coherent beams having the same intensities as the measured probe and conjugate beams, therefore in our case $\Delta^2\hat{n}_{\mathrm{SNL}} = \langle\hat{n}_a\rangle + \langle\hat{n}_b\rangle$. With the measured FWM gain and optical losses, theoretical curves shown in Fig. 4(b) in the main text can be thus readily plotted.

III. SBS INTENSITY GAIN PARAMETER ξ AND SIGNAL MAGNITUDE ESTIMATION

The SBS signal after interaction length L can be written as

$$\mathrm{I_{out}} = \mathrm{I_{probe}} \cdot e^{g_0\mathrm{I_{pump}L}}, \tag{11}$$

where g_0 is the maximal SBS gain [5]. In our experiment, $g_0 = 0.048$ m/GW [1], $\mathrm{L} \cong 2z_{\mathrm{R}} \cong 70$ μm, where z_{R} is the Rayleigh range as the signal comes almost entirely from the region where the intensity is the largest, and $\mathrm{I_{pump}} \sim 1.2$ GW/m^2 given the experimentally achievable maximal pump power of 36 mW and $1/e^2$ beam waist of 6 μm at the focal point. This yields $g_0\mathrm{I_{pump}L} = 4.2 \times 10^{-6}$. Therefore

$$\mathrm{I_{out}} = \mathrm{I_{probe}} \cdot e^{4.2\times10^{-6}} \cong (1 + 4.2 \times 10^{-6}) \cdot \mathrm{I_{probe}} = \mathrm{G_{SBS}} \cdot \mathrm{I_{probe}}. \tag{12}$$

Since we define in the main text that $\xi = \mathrm{G_{SBS}} - 1$, thus $\xi = 4.2 \times 10^{-6}$, which is within the range indicated by the gray bar in Fig. 4(b) in the main text.

Since $\mathrm{I_{out}} = (1 + 4.2 \times 10^{-6}) \cdot \mathrm{I_{probe}} = \mathrm{I_{probe}} + 4.2 \times 10^{-6} \cdot \mathrm{I_{probe}} = \mathrm{I_{common\ mode}} + \mathrm{I_{signal}}$, by using a balanced detector, the common mode intensity $\mathrm{I_{probe}}$ is rejected, therefore we see that the maximum SBS signal going into the detector is 4.2×10^{-6} of the total probe power (750 μW) going into the detector. The balanced detector has an electronic gain of $\sim 10^5$ V/W, therefore this SBS signal is $\sim 4.2 \times 10^{-6} \times 750 \times 10^5 = 315$ μV. As shown by the highest point in Fig. 2(b) in the main text, this estimation agrees with the measurement very well.

IV. DERIVATION OF THE RELATIONSHIPS BETWEEN SNR AND THE PUMP AND PROBE OPTICAL POWERS

In this section, we derive the relationship between the SNR (in dB) and the pump power (in dBm) of the SBS process. From Eq. (11), we see that when $g_0 \mathrm{I_{pump}} \mathrm{L} \ll 1$,

$$\mathrm{I_{out}} = \mathrm{I_{probe}} \cdot e^{g_0 \mathrm{I_{pump}} \mathrm{L}} \cong \mathrm{I_{probe}} \cdot (g_0 \mathrm{I_{pump}} \mathrm{L}) = \alpha \cdot \mathrm{I_{probe}} \cdot \mathrm{I_{pump}}, \tag{13}$$

with constant $\alpha = g_0 \mathrm{L}$. This relationship is demonstrated in Fig. 2(b) in the main text by keeping $\mathrm{I_{pump}}$ unchanged. If we write noise on the SBS signal as

$$\Delta \mathrm{I_{out}} = \beta \cdot \sqrt{\mathrm{I_{probe}}}, \tag{14}$$

where β is the noise factor, then for coherent excitation $\beta_{\mathrm{coh}} = 1$, while for squeezed excitation $\beta_{\mathrm{sqz}} < 1$. The SNR of this SBS signal registered by a RF spectrum analyser can thus be written as

$$\begin{aligned}
\mathrm{SNR[dB]} &= 10 \times \log_{10}(\frac{\mathrm{I_{out}}}{\Delta \mathrm{I_{out}}})^2 && (15)\\
&= 10 \times \log_{10}(\frac{\alpha \cdot \mathrm{I_{probe}} \cdot \mathrm{I_{pump}}}{\beta \cdot \sqrt{\mathrm{I_{probe}}}})^2 && (16)\\
&= 20 \times \log_{10}(\mathrm{I_{pump}}) + 10 \times \log_{10}(\frac{1}{\beta^2} \cdot \alpha^2 \mathrm{I_{probe}}) && (17)\\
&= 10 \times \log_{10}(\mathrm{I_{probe}}) + 10 \times \log_{10}(\frac{1}{\beta^2} \cdot \alpha^2 \mathrm{I_{pump}^2}). && (18)
\end{aligned}$$

Therefore for a fixed probe power (i.e., $\alpha^2 \mathrm{I_{probe}}$ is a constant), the SNR has a linear dependence on $10 \times \log_{10}(\mathrm{I_{pump}})$ (i.e., pump power in the unit of dBm) with a slope of 2. On the other hand, for a fixed pump power (i.e., $\alpha^2 \mathrm{I_{pump}^2}$ is a constant), the SNR has a linear dependence on $10 \times \log_{10}(\mathrm{I_{probe}})$ (i.e., probe power in the unit of dBm) with a slope of 1. These linear behaviors are demonstrated in Figs. 4(a) and (b) respectively in the main text. It is also worth noticing that information about the noise factor β is contained in the second terms of Eqs. (17) and (18). In our case, the quantum advantage of using squeezed light for the SBS spectroscopy over coherent light would be simply the differences between the two second terms,

$$\begin{aligned}
\text{Quantum Advantage [dB]} &= 10 \times \log_{10}(\frac{1}{\beta_{\mathrm{sqz}}^2} \cdot \alpha^2 \mathrm{I_{probe}}) - 10 \times \log_{10}(\frac{1}{\beta_{\mathrm{coh}}^2} \cdot \alpha^2 \mathrm{I_{probe}}) && (19)\\
&= 10 \times \log_{10}(\frac{1}{\beta_{\mathrm{sqz}}^2} \cdot \alpha^2 \mathrm{I_{pump}^2}) - 10 \times \log_{10}(\frac{1}{\beta_{\mathrm{coh}}^2} \cdot \alpha^2 \mathrm{I_{pump}^2}) && (20)\\
&= -20 \times \log_{10}(\beta_{\mathrm{sqz}}), && (21)
\end{aligned}$$

which in our case are 3.36 dB and 3.44 dB calculated from the two fits in Figs. 4(a) and (b) respectively in the main text.

V. IMAGE ACQUISITION TIME AND SPATIAL RESOLUTION IMPROVEMENT

As stated in the main text, acquiring the water SBS gain spectrum from 4 GHz to 6 GHz (with 40 MHz spectral resolution) in Fig. 5(b) took about 100 s, which is mainly limited by the *'write'* and *'read'* time of the instrument-computer interface, i.e., one needs to wait for at least 2 s for the spectrum analyzer to write the trace to its memory before the computer can view/read from it.

The quantum enhanced SBS spectra shown in Fig. 3 were obtained with 10 KHz resolution bandwidth, 10 Hz video bandwidth, and 1 s sweep time to scan a frequency span of 150 KHz (from 625 KHz to 775 KHz). In fact, one can significantly speed up the sweep time by using the *'zero span'* mode of the spectrum analyzer in conjunction with reducing the resolution bandwidth or increasing the video bandwidth. In our case, the sweep time can be reduced down to 2.4 ms while the spectrum analyzer is running in the 'zero span' mode with 3 KHz resolution bandwidth and 300 Hz video bandwidth.

To prove that our scheme also works with a much faster sweep time, we have retaken the SBS images of the glass triangle with the 'zero span' mode aforementioned, they turned out to be essentially the same as the ones shown in Fig. 6 (but are noisier since the video bandwidth is 30× wider). This implies that, our seemly slow acquisition rate is *not fundamentally limited by our scheme itself*, but is rather technically limited by the instrument. This technical limitation can be readily circumvented by the use of a more advanced RF spectrum analyzer (i.e., a real-time spectrum analyzer) having a much faster data writing and read-out rate, or having a large memory that data can be processed *locally*, so that the acquisition time would be solely limited by the sweep time of the spectrum analyzer. Therefore with a real-time spectrum analyzer our acquisition time would be 240 ms per 4 GHz spectrum (with 40 MHz spectral resolution), which is 120× slower than the state-of-art acquisition rate (20 ms per 4 GHz spectrum with 39 MHz spectral resolution for 'real' biological tissues, in pure water or homogenous liquids/solid, it would only require 2 ms per 4 GHz spectrum at a signal-to-noise ratio of 20 dB) reported in Ref. [8]. Whereas, the acquisition time in Ref. [8] was obtained with a total near-infrared excitation power of 265 mW, though they did not specify their pump and probe powers separately. In our set up the pump and probe powers are 7.5 mW and 750 μW respectively, thus the total excitation power in our scheme is only 8.25 mW in the infrared (795 nm).

It is also important to point out that in addition to showing an 'SNR image', it would be more useful to acquire images of practically relevant properties, such as the Brillouin frequency shifts and linewidths of the sample. This would more readily connect to real biological applications of SBS, as it is more informative of mechanical properties of the sample. In order to obtain these images, the entire spectrum must be acquired at each pixel, and then fitted for peak positions and linewidths. This, however, would require a lot longer acquisition times than the above stated.

With regard to the spatial resolution, it is very important to note that we chose to use the $f = 16$ mm plano-convex lenses to focus the probe and pump beams on the sample due to concerns of loss and alignment. Objectives would be able to focus the beams much more tightly, but would also introduce much more loss that the quantum advantage would be inevitably severely degraded. A practical straightforward resolution improvement under our current situation is to use molded aspheric lenses to focus the two beams on the sample. For example, using an aspheric lens with effective focal length $f = 4.5$ mm would yield a focal spot size ($1/e^2$) of 1.5 μm in diameter given our beam diameter ($1/e^2$) at lens is 3 mm. Although this would improve our resolution by a factor of 3, alignment would be much more challenging as one has to overlap the pump and prove beams within an excitation volume with 1.5 μm in diameter and 4.5 μm in length.

[1] R. W. Boyd, *Nonlinear Optics* (Academic Press, Burlington, MA, 2008).

[2] F. Li, T. Li, M. O. Scully, and G. S. Agarwal, Quantum advantage with seeded squeezed light for absorption measurement, Phys. Rev. Applied **15**, 044030 (2021).

[3] C. F. McCormick, A. M. Marino, V. Boyer, and P. D. Lett, Strong low-frequency quantum correlations from a four-wave-mixing amplifier, Phys. Rev. A **78**, 043816 (2008).

[4] T. Li, F. Li, C. Altuzarra, A. Classen, and G. S. Agarwal, Squeezed light induced two-photon absorption fluorescence of fluorescein biomarkers, Applied Physics Letters **116**, 254001 (2020).

[5] C. W. Ballmann, J. V. Thompson, A. J. Traverso, Z. Meng, M. O. Scully, and V. V. Yakovlev, Stimulated brillouin scattering microscopic imaging, Scientific Reports **5**, 1 (2015).

[6] F. Li, T. Li, and G. S. Agarwal, Experimental study of decoherence of the two-mode squeezed vacuum state via second harmonic generation, Phys. Rev. Research **3**, 033095 (2021).

[7] T. Li, B. E. Anderson, T. Horrom, B. L. Schmittberger, K. M. Jones, and P. D. Lett, Improved measurement of two-mode quantum correlations using a phase-sensitive amplifier, Opt. Express **25**, 21301 (2017).

[8] I. Remer, R. Shaashoua, N. Shemesh, A. Ben-Zvi, and A. Bilenca, High-sensitivity and high-specificity biomechanical imaging by stimulated brillouin scattering microscopy, Nature Methods **17**, 913 (2020).